Functional Kinomics Identifies Candidate Therapeutic Targets in Head and Neck Cancer

Russell Moser, Chang Xu, Michael Kao, et al.

Clin Cancer Res 2014;20:4274-4288.

Cancer Therapy: Preclinical
See related commentary by Bauman and Chung, p. 4173

Clinical Cancer Research

Functional Kinomics Identifies Candidate Therapeutic Targets in Head and Neck Cancer

Russell Moser[1], Chang Xu[2,3], Michael Kao[2], James Annis[4], Luisa Angelica Lerma[2], Christopher M. Schaupp[5], Kay E. Gurley[1], In Sock Jang[6], Asel Biktasova[7], Wendell G. Yarbrough[7], Adam A. Margolin[6], Carla Grandori[1,4], Christopher J. Kemp[1], and Eduardo Méndez[2,3,8]

Abstract

Purpose: To identify novel therapeutic drug targets for p53-mutant head and neck squamous cell carcinoma (HNSCC).

Experimental Design: RNAi kinome viability screens were performed on HNSCC cells, including autologous pairs from primary tumor and recurrent/metastatic lesions, and in parallel on murine squamous cell carcinoma (MSCC) cells derived from tumors of inbred mice bearing germline mutations in *Trp53*, and p53 regulatory genes: *Atm*, *Prkdc*, and $p19^{Arf}$. Cross-species analysis of cell lines stratified by p53 mutational status and metastatic phenotype was used to select 38 kinase targets. Both primary and secondary RNAi validation assays were performed on additional HNSCC cell lines to credential these kinase targets using multiple phenotypic endpoints. Kinase targets were also examined via chemical inhibition using a panel of kinase inhibitors. A preclinical study was conducted on the WEE1 kinase inhibitor, MK-1775.

Results: Our functional kinomics approach identified novel survival kinases in HNSCC involved in G_2–M cell-cycle checkpoint, SFK, PI3K, and FAK pathways. RNAi-mediated knockdown and chemical inhibition of the WEE1 kinase with a specific inhibitor, MK-1775, had a significant effect on both viability and apoptosis. Sensitivity to the MK-1775 kinase inhibitor is in part determined by p53 mutational status, and due to unscheduled mitotic entry. MK-1775 displays single-agent activity and potentiates the efficacy of cisplatin in a p53-mutant HNSCC xenograft model.

Conclusions: WEE1 kinase is a potential therapeutic drug target for HNSCC. This study supports the application of a functional kinomics strategy to identify novel therapeutic targets for cancer. *Clin Cancer Res; 20(16); 4274–88. ©2014 AACR.*

Introduction

Patients with head and neck squamous cell carcinoma (HNSCC) are treated aggressively with surgery followed by radiation, often together with cisplatin (1). Although these treatments increase loco-regional control, they are frequently disfiguring and induce high-grade toxicities limiting their effectiveness (2). Furthermore, resistance to cisplatin and radiation contributes to tumor recurrence, and options for those who do not respond are limited to palliative care. Targeted therapies for HNSCC are currently limited to experimental agents targeting the EGF receptor (3).

Mutations in the tumor-suppressor gene p53 are very common in HNSCC, with an estimated frequency of >50% (4, 5). Mutations in p53 have been associated with metastasis, resistance to radiation, and poor patient survival (6–8). Despite the strong implication of p53 in the biology and clinical outcome of HNSCC, there are no available therapies that specifically target p53-mutant cancer cells.

Here, we hypothesized that HNSCC cancer cells, in particular those with p53 mutations, are dependent on particular kinases for survival and that targeting these kinases

[1]Division of Human Biology, Fred Hutchinson Cancer Research Center, Seattle, Washington. [2]Department of Otolaryngology: Head and Neck Surgery, University of Washington Medical Center, Seattle, Washington. [3]Division of Clinical Research, Fred Hutchinson Cancer Research Center, Seattle, Washington. [4]Quellos High Throughput Facility, Institute for Stem Cell And Regenerative Medicine, University of Washington Medicine Research, Seattle, Washington. [5]Toxicology Program, Department of Environmental and Occupational Health Sciences, University of Washington, Seattle, Washington. [6]Sage Bionetworks, Seattle, Washington. [7]Deparment of Surgery, Otolaryngology: Head and Neck Surgery, Yale University School of Medicine, New Haven, Connecticut. [8]Surgery and Perioperative Care Service, VA Puget Sound Health Care System, Seattle, Washington.

Note: Supplementary data for this article are available at Clinical Cancer Research Online (http://clincancerres.aacrjournals.org/).

R. Moser and C. Xu contributed equally to this article.

Corresponding Authors: Eduardo Méndez and Christopher J. Kemp, Fred Hutchinson Cancer Research Center, 1100 Fairview Avenue North, Seattle, WA 98109. Phone: 206-667-2625; Fax: 206-667-5765; E-mail: edmendez@u.washington.edu; cjkemp@fhcrc.org

doi: 10.1158/1078-0432.CCR-13-2858

Translational Relevance

In this study, we address the unmet need to find novel therapies for p53-mutant head and neck squamous cell carcinoma (HNSCC). We used a functional kinomics approach and human–murine interspecies comparison of high-throughput siRNA viability screens to identify conserved survival pathways in SCC. The rationale for targeting kinases in cancer is significant, and as such we focused on the kinome to identify druggable and clinically relevant survival kinases in HNSCC. Our findings reveal vulnerabilities of p53-mutant HNSCC cells to inhibition of G_2–M, SFK, PI3K, and FAK pathways. For proof-of-concept and mechanism, we performed preclinical validation studies on one of our top kinase targets, WEE1. Our preclinical data demonstrate the vulnerability of p53-mutant HNSCC cells to deregulation of the G_2–M transition, and support initiation of clinical trials with MK-1775 or other G_2–M checkpoint inhibitors for HNSCC, particularly in combination with cisplatin.

could have therapeutic potential. To identify these cancer-specific survival kinases, we used an unbiased and genome scale high-throughput siRNA gene–silencing strategy. We surveyed the entire human kinome to identify those kinases that are required for survival of HNSCC cells stratified by p53 mutational status and metastatic propensity. We included pairs of HNSCC cells derived from primary tumors and either recurrent or metastatic lesions. The cell lines derived from the recurrent or metastatic tumors have been shown by us and others to have more aggressive features than their primary tumor autologous pairs, as measured by migration, avoidance of anoikis, and metastatic potential in mouse orthotopic xenografts (Materials and Methods for details; ref. 9). Recurrent metastatic tumors are generally resistant to standard-of-care therapies and as such are most in need of novel targeted therapies.

The rationale for targeting kinases in human cancer is significant. These enzymes regulate multiple cellular processes that contribute to tumor development and progression, and many human tumors display aberrant activation of kinases caused by genetic alterations. For tumors that are dependent on kinase activity for survival, targeted drugs could be effective.

Understanding that human cancer cell lines exhibit genetic and phenotypic heterogeneity, which can hamper the identification of robust drug targets, we performed a parallel siRNA kinome screen using a set of low passage murine squamous cell carcinoma (MSCC) cells. These cancer cells were derived from tumors of inbred mice bearing germline mutations in *Trp53* and p53 regulatory genes *Atm*, *Prkdc*, and $p19^{Arf}$ (10–13). This set of p53 pathway-deficient cancer cells share the same culture history and genetic background and were derived from tumors sharing the same etiology. Comparative analysis of siRNA screen results between mouse and human cells identified kinases relevant to SCC survival. We reasoned that these evolutionarily conserved kinases might represent more robust therapeutic targets. Through an efficient *in vitro* and *in vivo* prioritization and validation scheme, we identified the G_2–M cell-cycle regulatory kinase WEE1 as one of several clinically promising targets, and show that inhibition of WEE1 with a highly specific small-molecule inhibitor impaired growth of p53-mutant HNSCC tumors *in vivo*.

Materials and Methods

Cell lines

The following human HNSCC cell lines were used: UM-SCC14A, UM-SCC14C, PCI-15A, PCI-15B, JHU-019, UM-SCC22A, UM-SCC22B, UM-SCC38, UM-SCC17A, SCC-61, and three HPV(+) cell lines: UM-SCC47, UPCI:SCC090, and UM-SCC104 (Supplementary Table S1). Three cell line pairs were derived from primary tumors and subsequent recurrences or metastatic cervical lymph nodes from the same patients: UM-SCC14A and UM-SCC14C; PCI-15A and PCI-15B; and UM-SCC22A and UM-SCC22B. The cell line JHU-019 was derived from a late-stage patient with oral SCC (Supplementary Table S1). For the paired lines, wound-healing assays revealed that the migration rate of cell lines derived from metastatic HNSCC (i.e., UM-SCC-14C and PCI-15B) was higher than those derived from the primary tumor (i.e., UM-SCC-14A and PCI-15A) and that JHU-019 had the fastest migration rate (9). In addition, JHU-019 and PCI-15B cell lines tested in mouse xenografts by orthotopic injection into the tongue produced squamous carcinoma at the sites of injection and cervical lymph node metastasis (9). Given a previous report raising concerns of JHU-019 contamination with prostate adenocarcinoma cells (14), we performed immunohistochemistry staining of 4 paraffin-embedded blocks from JHU-019 tumors orthotopically-injected in the tongue of NOD/SCID IL2 gamma null mice (NSG) with antibodies against 3 markers used clinically to identify both squamous cell and prostate carcinoma (EP1601Y for Cytokeratin 5 (CK5); BC4A4 for p63; and PSA for Prostate Specific Antigen). Staining and evaluation of the immunohistochemical stains cited above were determined by the CLIA-certified UW Medicine Pathology Laboratories. There was uniformly positive staining for p63 in all blocks, uniformly positive staining for CK5 in two blocks and variably positive staining in the other two blocks. There was no staining for PSA in any of the blocks (data not shown). To determine p53 mutational status, we designed primers to amplify exons 2-11 using Primer3 software (Whitehead Institute, Cambridge, MA). Primer specificity was confirmed by gel electrophoresis. PCR-amplified fragments were purified and sequenced using an ABI 3730xl DNA Analyzer with ABI's BigDye Terminator Cycle Sequencing method. Sequencing results are aligned to GenBank TP53 sequence NG_017013.1 using Sequencher 4.10.1 (Gene Codes, Ann Arbor, MI). Cell lines were characterized for metastatic potential as described (9). To determine if a p53 mutation is disruptive, we used criteria established by Poeta *et al.* (7).

MSCC cells were derived from NIH/Ola strain mice with germline mutations in p53 pathway genes and

included: MSCC-CK101 ($Hras^{Q61L}$ $Trp53^{+/+}$), MSCC-CK102 ($Hras^{Q61L}$ $Trp53^{+/-}$), MSCC-CK103 ($Hras^{wt}$ $p19Arf^{-/-}$), MSCC-CK104 ($Kras^{G13R}$ $Atm^{-/-}$), MSCC-CK1 ($Hras^{Q61L}$ $p53^{+/+}$), and MSCC-CK4 [$Hras^{Q61L}$ $p53^{-/-}$ ($Cre+$ $p53$ lox/lox); refs. 10–12]. MSCC-CK105 ($Hras^{Q61L}$ $Prkdc^{mu/mu}$) cells were from SCID-mutant mice of a mixed C3H/Balb/c background (Supplementary Table S2) (13). All mice were subjected to the identical DMBA/TPA (7,12-dimethylbenz(a)anthracene/12-O-tetradecanoylphorbol-l3-acetate) two-stage carcinogen protocol to induce SCC. Tumors induced by this protocol principally harbor an activating mutation in the *Hra*s oncogene, but mutations in *Kras* have also been noted (15, 16). Carcinomas arising from both $p19^{Arf}$- and p53-deficient mice are highly aggressive and metastatic (11, 12, 17, 18). Mouse SCC lines were derived using a standard outgrowth explant method. Briefly, carcinoma tissue was washed in sterile PBS, sliced into 2-mm pieces using a sterile razor blade, and placed into a 60-mm tissue culture plate with Dulbecco's Modified Eagle Medium, 10% fetal calf serum and penicillin/streptomycin. Media were replaced every 72 hours until cell outgrowths reached 70% to 90% confluence, and were subsequently passaged and/or frozen at low passage number. Total RNA was isolated from the MSCC-CK1 line with TRizol and cDNA generated using Superscript 3 reverse transcriptase (Life Technologies). The p53 cDNA transcript spanning exons 2 to 11 was PCR amplified as previously described (19), and cloned into a TOPO TA vector (Life Technologies), competent cells transformed, and several colonies sequenced using an ABI 3730xl DNA Analyzer with the ABI's BigDye Terminator Cycle Sequencing method for mutations in the *p53* gene (Supplementary Table S2).

High-throughput RNA interference kinome screens

Kinome-wide siRNA screens were performed with viability as the phenotypic endpoint on five HNSCC lines: JHU-019; PCI15A and 15B; UM-SCC14A and 14C; and five MSCC lines: MSCC-CK101, MSCC-CK102, MSCC-CK103, MSCC-CK104, and MSCC-CK105. Normal human foreskin fibroblasts (HFF) were screened to control for nonspecific cell toxicity (UW-Quellos facility proprietary data). Briefly, culturing of normal HFFs was performed as previously described (20). Kinome-wide RNA interference screens were performed on two cultures of HFFs (HFF1, HFF3) using the Ambion kinome library (Ambion-Life Technologies). An HFF exclusion plot was generated using this kinome screen information to determine whether RNAi-mediated knockdown of kinase targets compromised cell viability in both HFF cultures, with <70% viability (>30% cell death) as a threshold (Supplementary Fig. S2; partial data shown). siRNA libraries targeting 713 human (MISSION siRNA Human Gene Family Set; Sigma) and 572 murine kinases (Ambion) were constructed and used in pools of three independent siRNAs targeting each gene, in a one gene per well approach. RNAi screens were performed in 384-well format using robotics instrumentation (21). Transfection feasibility of each cell line was established using a factorial optimization. Mock condition and a nontargeting universal siRNA control were used as negative controls, whereas an siRNA directed at KIF11 (kinesin-like protein), which arrests cells in mitosis, was used as a positive control. All reagent conditions were statistically evaluated using a simple *Z*-factor score to evaluate differentials and variability of replicates (i.e., potent cell killing with KIF11 at the lowest toxicity possible in the mock universal controls) to select an optimized transfection condition for each cell line (22). All kinases were tested in triplicate to establish experimental variability and statistical validity. Scrambled siRNA-negative controls were used to monitor dynamic range and off-target effects and the results were standardized to mock-transfected cells. Viability and apoptosis were quantified using an Envision Multilabel detector/plate reader (PerkinElmer) with either a CellTiter-Glo assay (Promega), or Apotox assay (Promega), the former measures metabolic ATP via a standard curve to mock/universal siRNA at all conditions. Raw luminescence values were mock normalized per plate and then *Z*-transformed per cell line and plotted for distribution and data mining (Miner 3D software; version 7.3). All high-throughput kinome screens and subsequent validation screens on MSCC and HNSCC cells were statistically evaluated using published methods (23).

Comparison of human and mouse kinome screens

The 713 human (Supplementary Table S3) and 572 murine kinase (Supplementary Table S4) sets were cross-referenced using mouse genome informatics (http://www.informatics.jax.org/) and National Center for Biotechnology Information (http://www.ncbi.nlm.nih.gov/) database nomenclature to generate a common list of 508 kinases referred to as the interspecies kinome (Supplementary Table S5). Using this common list, prioritization of screen results then followed on the basis of the viability scores from the five HNSCC cells and five MSCC cell lines. Mean viabilities (μ_{i2}) from five HNSCC cell lines [$\mu_{i2\ \mathrm{All\ (human)}} = \mu_i\,(\mathrm{O19}) + \mu_i\,(14\mathrm{A}) + \mu_i\,(14\mathrm{C}) + \mu_i\,(15\mathrm{A}) + \mu_i\,(15\mathrm{B})$] and from five MSCC cell lines were calculated [$\mu_{i2\ \mathrm{All\ (murine)}} = \mu_i$ (wild-type) + μ_i ($Trp53^{+/-}$) + μ_i ($p19^{Arf-/-}$) + μ_i ($Atm^{-/-}$) + μ_i (*Prkdc* mu/mu)] for each of 508 kinases $\{i = 1, 2, 3, 4, \ldots, 508\}$, where μ_i is the triplicate of pooled siRNAs (three distinct siRNAs) average normalized viability for each individual gene per cell line. Mean viabilities (μ_{i2}) for each gene were then *Z*-transformed using the equation, $Z = \mu_{i2} - \mu/\sigma$, where μ is the mean viability and σ the SD for all siRNAs per wells for all five HNSCC cell lines and all five MSCC cell lines, respectively (Supplementary Table S8). Mean viabilities ($\mu_{i2\ \mathrm{All}}$, $\mu_{i3\ \mathrm{p53\ mutant}}$, $\mu_{i4\ \mathrm{metastatic}}$) and *Z*-score transformations were calculated for both human and murine lines per genotype and phenotype: (i) all human and murine cell lines; (ii) p53-mutant/deficient human and murine cell lines; and (iii) metastatic human and murine cell lines (Supplementary Table S8). Cartesian plots ($Z\text{-score}_{murine}$, $Z\text{-score}_{human}$) of all 508 kinases in common with murine and human kinomes were then generated for each of the three comparisons. Population mean viabilities ($\mathrm{Mean_{All}}$, $\mathrm{Mean_{p53\ mutant\ All}}$,

$Mean_{Met}$) and *Z*-score transformations ($Z\text{-score}_{Mean\ All}$, $Z\text{-score}_{p53\ mutant\ All}$, $Z\text{-score}_{Mean\ Met}$) were calculated for specific genotypic and phenotypic comparisons and used in the color-coded overlay on the cartesian plots for selection per comparison (Fig. 1B; Supplementary Table S8). Kinase targets were selected on the basis of *Z*-score threshold from each of the cartesian plots: $Z\text{-score}_{mean\ All} < -1.0$; $Z\text{-score}_{p53\ mutant\ All} < -2.0$, $Z\text{-score}_{Mean\ Met} < -1.5$ (Supplementary Table S8), in which kinases were data mined from more then one comparison and duplicates were removed for a final selection of 38 kinase targets from all three comparisons, kinase targets (38 kinases) = kinase $targets_{All}$ + kinase $targets_{p53mutant}$ + kinase $targets_{Met}$ (Fig. 1B and C; Supplementary Table S8). Kinases were further prioritized on the basis of those whose expression or activity was increased in SCC and that play known functions in SCC pathogenesis.

Primary validation of kinase targets with siRNA

Twenty-eight kinases were selected for follow-up and validation based on the interspecies kinome comparison and HFF kinase exclusion. Two small-scale time-course primary validation RNAi screens were performed in parallel on four HNSCC cell lines (UM-SCC14A, UM-SCC14C, PCI-15A, and PCI-15B) in 384-well formats with an independent set of siRNAs (Qiagen; Supplementary Table S6), with three separate siRNAs plus pooled siRNAs per gene target in triplicate for an $N = 12$ for each gene target. All phenotypic endpoints of cell viability and caspase-3/7–dependent apoptosis were measured in parallel screens in a time-course format at 1.5, 3, and 4.5 days posttransfection using the CellTiter-Glo assay (Promega) and Apotox-Glo (CaspaseGlo-3/7 reagent) assay (Promega) per the manufacturer's specifications and an Envision multilabel plate reader (PerkinElmer). Primary screen "hits" were assessed using a single endpoint for cell viability at 4.5 days posttransfection termed, absolute viability, by both a negative control–independent analysis: triplicate siRNAs versus population mean of the screen, *Z*-score threshold and the unpaired *t* test, *Z*-score < -1.0, $P < 0.1$ scored as hit (Supplementary Table S13; Column U), as well as a negative control–dependent analysis: triplicate siRNAs versus universal negative control siRNAs, ANOVA with Dunnetts posttest, mean difference >0 and $P < 0.05$ scored as hit (Column AA; Summary of "hits"; Supplementary Tables S13 and S14). Comparing posttransfection effects on absolute viability (day 4.5) for each kinase target with either the universal negative control siRNA or the population mean yielded similar results (Supplementary Tables S13 and S14). Differential viabilities (days 4.5–1.5) based on the mean of both the $N = 12$ data (i.e., all three distinct siRNAs per target plus pooled siRNAs in triplicate) and $N = 3$ data (i.e., pooled siRNAs alone) were calculated for all 28 kinase targets (Supplementary Tables S10–S12). AUC (area under the curve) estimates of caspase-dependent apoptosis ($AUC_{estimate}$) using all three data points with both the $N = 12$ data and $N = 3$ pooled siRNAs were calculated for all kinase targets (Supplementary Tables S15–S17). Statistical significance of RNA interference–mediated knockdown of the 28 kinases was assessed via ANOVA with Dunnetts posttest for multiple comparisons ($P < 0.05$ as significant) on differential viability (days 4.5–1.5), and AUC analysis of caspase-3/7–dependent apoptosis versus universal negative siRNA control; Supplementary Tables S10–S12 and S15–S17).

Secondary validation of kinase targets with siRNA

Ten kinase targets were further validated in a 96-well format in five additional HNSCC cell lines (UM-SCC22A, UM-SCC22B, UM-SCC38, UM-SCC47A, and JHU-019). In addition, the 10 HFF exclusion kinase targets were included in the low-throughput assay (i.e., 20 kinase targets). This assay consisted of three independent siRNAs per well (pooled siRNAs) assayed in triplicate (Qiagen; Supplementary Table S7) for cell viability and apoptosis measured at 1.5, 3, and 4.5 days posttransfection using the Apotox-Glo assay (Promega) as per the manufacturer's specifications using a Synergy H4 Hybrid Multi-Mode microplate reader (BioTek). Statistical significance of RNA interference–mediated knockdown of the 20 kinases was assessed via ANOVA with Dunnetts posttest for multiple comparisons on absolute viability (day 4.5), differential viability (days 4.5–1.5), and AUC analysis of caspase-dependent apoptosis versus the negative siRNA control (Supplementary Tables S18–S20).

Dose–response curves with kinase inhibitors

Kinase inhibition dose–response curves were performed with six kinase inhibitors [MK-1775 (a.k.a., AZD-1775), TAE684, PI828, PIK93, PP2, and PF-562271] against kinase targets [WEE1, ALK, PI3K, PIK4CB, FYN, and FAK (ILK surrogate)], respectively. Kinase inhibitors: MK-1775 (S1525), PIK93 (S1489), and TAE684 (S1108) were obtained from Selleck Chemicals; PI828 (2814), PP2 (1407) from Tocris Bioscience, and PF-562271 from SYNkinase. All HNSCC (UMSCC-17A, UM-SCC47A, PCI-15A, PCI-15B, UM-SCC14A, and UM-SCC14C) and MSCC (CK1, $p53^{+/+}$ and CK4, $p53^{-/-}$) cells were plated at approximately 5 to 10×10^3 cells per 100 μL per well, and incubated at 37°C for approximately 24 hours on 96-well assay plates (Corning Inc.). Serial dilutions of the kinase inhibitors and vehicle control (dimethyl sulfoxide, DMSO) were prepared in 1 mL assay blocks at 3× working concentration to generate dose–response curves ranging from 100 to 0.03 μmol/L. All serial dilutions were prepared using cell culture media. Approximately 72 hours after treatment, cells were assessed for metabolic activity via ATP using CellTiter-Glo (Promega), following the protocol outlined by the manufacturer using an FLx800, and/or a Synergy H4 Hybrid multimode reader (BioTek). All assays were performed in triplicate and normalized to wells with no treatment. Dose–response curves and IC_{50} values were generated using GraphPad Prism Version 5 [parameters, nonlinear regression fit; equation = log (inhibitor) vs. response − variable slope (four parameters); single constraint].

COSMIC public database of drug sensitivity data

Using the Catalogue of Somatic Mutations in Cancer (COSMIC) website, TP53 gene mutational status was extracted from the Sanger Cancer Cell Line Project, which contains information on 820 cancer cell lines. In addition, the genomics of the Drug Sensitivity Project (released July 2, 2012) contains 541 cancer cell lines that were treated with a WEE1/CHK1 inhibitor, 681640 (EMD Millpore), a pyrrolocarbazole compound that acts as a potent, ATP-binding site inhibitor of WEE1 ($IC_{50} = 11$ nmol/L). Drug sensitivity was measured with nine different concentrations of 681640 and IC_{50} values presented as natural log (μmol/L; Supplementary Table S21). The sign test was applied to test the median difference in sensitivity by TP53 status. We performed a similar analysis on only the SCC cell lines. Forty-two squamous cell lines were identified from COSMIC annotation, eight were p53 wild-type and the remaining 34 had a p53 mutation.

Mitotic entry, cell-cycle analysis, and apoptotic assays

Mitotic entry was assessed as previously described (24). Briefly, HNSCC cells (PCI-15B, UMSCC-17A) were treated with 1 μmol/L MK-1775 for 8 and 24 hours, and all cells were harvested, washed, and incubated with rabbit monoclonal antibody to phospho-histone H3 (Serine10; Cell Signaling Technology; Cat. no. 3465) for 2 hours at room temperature, washed, and DNA stained with 20 μg/mL propidium iodide, RNaseA in PBS (Sigma-Aldrich; Cat. nos. P4170, R6513). Flow cytometric analysis was performed using a BD FACS Canto II, and profiles analyzed with BD Cell Quest software (Becton Dickinson). Caspase-3/7–dependent apoptosis was assessed as per the protocol (Promega; Cat. no. G8091) using a SynergyH4 Hybrid Reader (BioTek). AUCs were calculated for all treatments and vehicle (DMSO) for all cell lines using two measurements over a 48-hour period with three concentrations (30 nmol/L, 100 nmol/L, and 1 μmol/L) of MK-1775.

NSG xenograft tumor model

PCI-15B cells were inoculated subcutaneously into the right flanks of 28 eight-week-old NOD/SCID interleukin-2 gamma (NSG) null mice provided by the Olson laboratory at the Fred Hutchinson Cancer Research Center (Seattle, WA). When tumors reached a palpable mass of >50 mm^3, mice were randomly assigned into four treatment groups of 7 mice each and all measurements and treatment regimens were carried out using a double-blind protocol. The WEE1 inhibitor MK-1775 (S1525-Selleck Chemicals) was delivered by oral gavage (30 mg/kg) twice per week for 4 weeks in DMSO in 0.5% methylcellulose (M0512; Sigma-Aldrich) in a 1:14 suspension. Cisplatin (P4394, cis-diammineplatinum (II) dichloride; Sigma-Aldrich) was delivered via intraperitoneal injection (4.0 mg/kg) once a week for 4 weeks. The volume of the implanted tumor was measured weekly with calipers and tumor volumes calculated using the formula: $V = L \times W^2/2$; in which V, volume (mm^3); L, largest diameter (mm); W, smallest diameter (mm). All animal protocols were approved by the Fred Hutchinson Cancer Research Center Laboratory Animal Care and Use Committee.

Immunoblotting

Tumor tissues were minced and homogenized on ice in M-PER Mammalian Protein Extraction Reagent supplemented with Halt Protease and Phosphatase Inhibitor Cocktail (Thermo Fisher Scientific). Extracted proteins were quantified by a bicinchoninic acid protein assay (Thermo Fisher Scientific). Fifty micrograms of each protein specimen was revealed on a NuPAGE 4% to 12% Bis-Tris mini gel (Life Technologies) and transferred onto an Immobilon-P polyvinylidene difluoride membrane (Millipore). Anti-WEE1 (Cat. no. 4936), anti–phospho-WEE1 (Ser642; Cat. no. 4910), anti-CDC2 (Cat. no. 9112), and anti–phospho-CDC2 (Tyr15; Cat. no. 4539) antibodies were purchased from Cell Signaling Technology. The secondary antibodies used were ZyMax horseradish peroxidase (HRP)–conjugated goat-anti-rabbit immunoglobulin G (Life Technologies). HRP was detected with the Super-Signal West Pico Chemiluminescent Substrate Kit (Thermo Fisher Scientific). Densitometry on immunoblot analysis was performed with ImageJ software (Wayne Rasband, NIH, Bethesda, MD) and raw data normalized to β-actin loading control per lane.

Statistical analysis

All column and curve data points presented as mean ± SEM, unless otherwise noted. All statistical analyses were performed using unpaired two-tailed t tests unless otherwise indicated. All statistical analysis of RNAi interference primary and secondary screening data is described above and all calculations used for significance testing are presented in Supplementary Tables. Statistical tests were all performed using GraphPad Prism versions 5 and 6 (GraphPad Software Inc.) (Supplementary Tables S9–S20).

Results

RNA interference kinome screens of SCC

We performed kinome-wide siRNA viability screens on a set of five HNSCC cell lines (UM-SCC14A; UM-SCC14C; PCI-15A; PCI-15B; and JHU-019). Two pairs of these cells (UM-SCC14A, UM-SCC14C and PCI-15A, PCI-15B) were derived from primary and subsequent posttreatment recurrences or metastatic cervical lymph nodes from the same patients and all carried mutations in p53 (Supplementary Table S1). A total of 713 kinases were interrogated using an arrayed siRNA platform that quantified cell viability following knockdown with a pool of three siRNAs per gene per well. All assays were performed in triplicate. Cell viability was monitored 4 days after siRNA transfection using the ATP-based, CellTiter-Glo assay (see Materials and Methods for details). In parallel, we performed kinome-focused screens on a set of five low passage cancer cells derived from MSCC (Supplementary Table S2). These cells were isolated from carcinoma-bearing inbred mice harboring germline

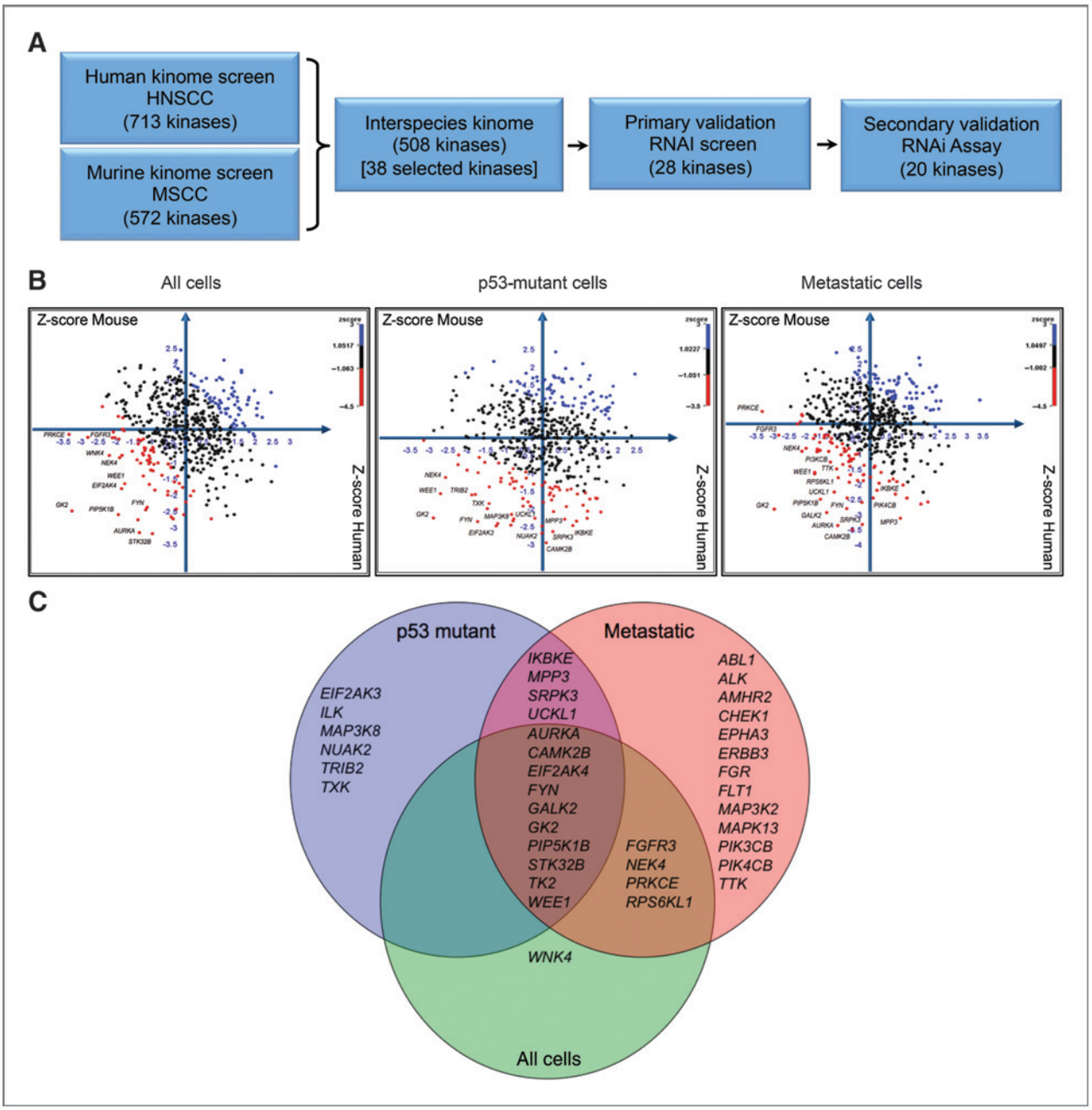

Figure 1. Comparative functional kinomics approach to identify survival kinases in SCC. A, flow chart schematic of functional kinomic approach for discovery of kinase targets. RNAi screen hits from both murine (MSCC) and human (HNSCC) cells were prioritized by cross-species comparison. B, Cartesian plots of *Z*-scores from interspecies kinome (508 kinases) to identify kinase targets that had the highest shared impact on cell viability. Human and mouse cell lines were sorted into each of three comparisons: All cells (left), p53-mutant cells (middle), and metastatic cells (right). Candidate kinase targets with *Z*-scores greater than one SD from the mean cell viability per comparison are shown in red; Supplementary Table S8 for details. C, the Venn diagram of selection of 38 kinase targets from interspecies comparison; inclusion in diagram represents kinases targets that met a certain threshold in each comparison.

mutations in the p53 pathway genes *Atm*, *Prkdc*, $p19^{Arf}$, and *Trp53* (10–13).

Next, we derived an interspecies kinome (508 kinases shared between both species) to identify kinases in which RNA interference–mediated knockdown negatively affected cell viability in both human and mouse cells (see schematic in Fig. 1A). Cell screens were further stratified by p53-mutant status and metastatic propensity. Cartesian plots with cross-species comparison of viability *Z*-scores for all 508 kinases, for all cell lines (left), p53-mutant cell lines (middle), and metastatic cell lines (right) are shown in Fig. 1B. Thirty-eight kinases were selected for follow-up based on several criteria, including shared negative *Z*-scores in both species and specificity to

cells with mutant p53 and metastatic phenotype (Fig. 1C; Supplementary Table S8). Many of these putative HNSCC survival kinases are implicated in signaling pathways such as focal adhesion and integrin signaling (CAMK2B, FYN, ILK, EPHA3, EIF2AK4, and TRIB2), PI3K (phosphoinositide 3-kinase) signaling (PIK4CB, PIK3CB, PIP5K1B, TRIB2, FGFR3, and ALK), SRC signaling (FYN, TXK, and CAM2KB), and G_2–M cell-cycle regulation (WEE1, NEK4, TTK, AURKA, and CHK1).

To prioritize targets for preclinical validation, we used primary cultures of HFFs to assess whether inhibition of these kinases caused toxicity to normal cells. Ten kinases caused >30% loss in cell viability in both HFF cultures (Supplementary Fig. S2) and were not included in the primary validation screen. The remaining 28 kinase targets were retested with independent siRNAs on the same two pairs of autologous HNSCC cell lines (UM-SCC14A and 14C; PCI-15A and 15B) using a format of three separate siRNAs per gene plus a pool of all three siRNAs, each in triplicate (i.e., $N = 12$/gene; Supplementary Fig. S1). Both cell viability and caspase-3/7–dependent apoptosis were measured in parallel at 1.5, 3, and 4.5 days posttransfection. Differential viability (days 4.5–1.5), absolute viability (day 4.5), and apoptosis was calculated for each kinase (Supplementary Tables S9–S17; Material and Methods for details). Differential viabilities were calculated to measure posttransfection effects over time (days 4.5–1.5) and statistically evaluated versus the universal negative control siRNA (Fig. 2A; Supplementary Tables S10–S12). Differential viabilities calculated using three separate siRNAs per gene plus the pool of all three siRNAs yielded comparable results with using the pool of all three siRNAs alone (Supplementary Tables S10–S12). We focused on the pooled analysis to reduce off-target effects (25). Likewise, results obtained using either differential or absolute viability metrics yielded similar prioritized kinase targets (Supplementary Tables S10–S14; see Materials and Methods for details). To measure the cumulative effects of RNAi-mediated knockdown on apoptosis, AUC estimates of caspase-dependent apoptosis were determined versus the universal negative control siRNA (Fig. 2B; Supplementary Fig. S1; Supplementary Tables S15–S17). Results from this primary validation screen revealed that many of the kinase targets that significantly reduced viability also increased apoptosis (Fig. 2A). RNAi-mediated knockdown of NEK4 and WEE1 kinases led to a significant reduction in cell viability in all four cell lines tested, whereas targeting TRIB2 did so for three of the four lines.

Ten kinase targets [NEK4, WEE1, ILK, CAM2KB, FGFR3, FYN, PI4KB (PIK4CB), TRIB2, TTK, and TXK] that caused a significant reduction in viability and/or increase in apoptosis following siRNA transfection in at least one cell line were selected for secondary validation on five additional HNSCC lines (UM-SCC22A, UM-SCC22B, UM-SCC47, and UM-SCC38, JHU-019), and kinase target metrics were measured and calculated using the same format as above (Supplementary Fig. S1 and Supplementary Tables S18–S20). UM-SCC22A and UM-SCC22B are an autologous pair of cells derived from a primary tumor and cervical lymph node metastasis from the same patient. We also retested 10 kinases from the discovery screen in which siRNAs reduced viability in HFFs (Fig. 2B; Supplementary Fig. S1; Supplementary Tables S1 and S18–S20).

RNAi-mediated knockdown of kinases that regulate the G_2–M transition, NEK4, WEE1, AURKA, and CHK1, as well as FYN and CAM2KB significantly impaired viability in three or more of the five cell lines tested (Fig. 2B), whereas knockdown of the WEE1, NEK4, and AURKA kinases induced the highest levels of apoptosis in all five HNSCC cell lines. Altogether, compiled primary and secondary validation data showed that RNA interference–mediated knockdown of WEE1, NEK4, and AURKA kinases significantly reduced viability and increased apoptosis in more than 75% of HNSCC cell lines (Fig. 2C).

A comparison of functional kinomic profiles between cell line pairs isolated from the same patients showed a high degree of concordance, but with a tendency for the metastatic/recurrent cells to be more resistant to kinase knockdown relative to their primary tumor cell pair (Fig. 2 and Supplementary Fig. S3). For example, RNAi-mediated knockdown of TK2 and TRIB2 was more effective in cells isolated from the primary versus the recurrent/metastatic lesions (Fig. 2A and Supplementary Fig. S3). Several kinases, such as WEE1 and NEK4, remained equally effective in both primary and recurrent/metastatic tumors.

Small-molecule inhibition of kinases confirms role in HNSCC cell survival

We further prioritized kinase targets using commercially available small-molecule inhibitors. This step not only provides independent chemical confirmation of siRNA results but also provides lead compounds to test in *in vivo* models. Dose–response curves using kinase inhibitors were performed for WEE1 (MK-1775), ALK (TAE684), PIK4CB (PIK93), FAK (PF-562271), PIK3CB (PI828), and FYN (PP2; Fig. 3). In agreement with our siRNA knockdown experiments, p53-mutant HNSCC cell lines were sensitive to small-molecule inhibitors targeting WEE1, ALK, PIK4CB, and FAK. The WEE1 kinase inhibitor, MK-1775 had the broadest and most significant effect on cell survival in both primary and recurrent/metastasis-derived HNSCC cells, with an IC_{50} ranging from 220 nmol/L to 3.1 μmol/L (Fig. 3).

Preclinical validation of WEE1 as a drug target for HNSCC *in vitro* and *in vivo*

Results from our cross-species comparative analysis of kinome screens, validation assays, and small-molecule inhibitor studies nominated WEE1, a G_2–M regulator, as a promising target against p53-mutant HNSCC. To further explore the sensitivity of p53-deficient cells to WEE1 inhibition, we performed dose–response curves with MK-1775 in pairs of p53 wild-type and p53-mutant/deficient SCC cells. The IC_{50} for MK-1775 was 20-fold lower in $p53^{-/-}$

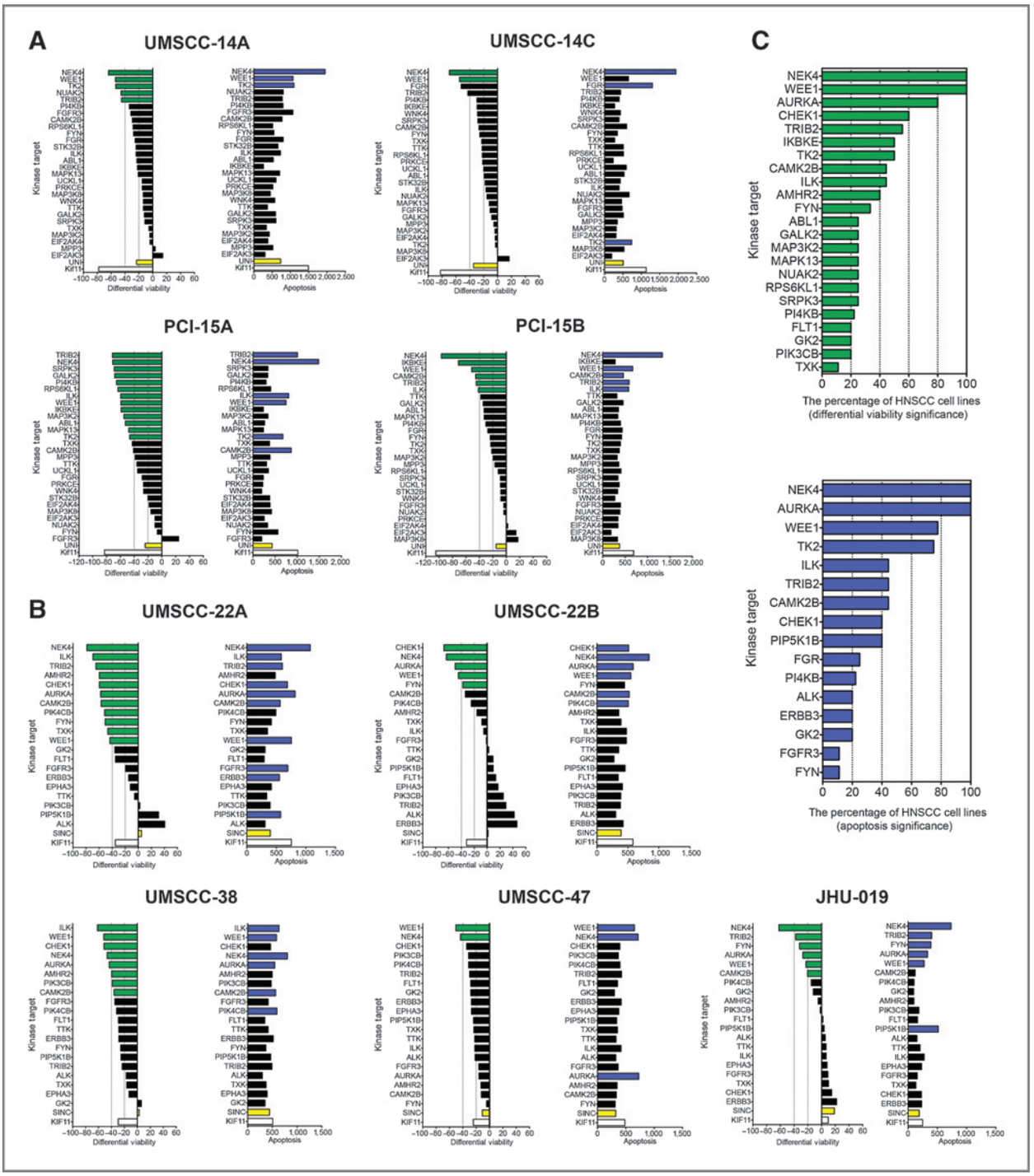

Figure 2. RNA interference validation screens on kinase targets. A, RNAi primary validation screen; left bar graphs, differential cell viability (days 4.5–1.5) of RNAi-mediated knockdown of 28 kinase targets in autologous pairs of HNSCC cell lines derived from primary tumor and recurrent/metastatic site (14A, 14C, 15A, and 15B); kinase target versus universal negative siRNA control (UNI in yellow), $P < 0.05$ (green); right bar graphs, caspase-dependent apoptosis integrated over 4.5-day time-course of RNAi-mediated knockdown of 28 kinase targets, kinase target versus UNI, $P < 0.05$ (blue); results ranked by differential viability for each kinase target per the HNSCC cell line. KIF11 positive control for differential viability (white). B, RNAi secondary validation assays in five additional HNSCC cell lines (22A, 22B, 38, 47, and 019); left bar graphs, differential cell viability (days 4.5–1.5) of RNAi-mediated knockdown of 20 kinase targets in HNSCC cell lines, kinase target versus the negative siRNA control (SINC in yellow), $P < 0.05$ (green); right bar graphs, caspase-dependent apoptosis integrated over 4.5-day time-course of RNAi-mediated knockdown of 20 kinase targets in HNSCC cell lines, kinase target versus SINC, $P < 0.05$ (blue), results ranked by differential viability for each kinase target per the HNSCC cell line. KIF11 positive control for differential viability (white). C, kinase target significance in HNSCC. RNAi-mediated knockdown of kinase targets ranked by the percentage of HNSCC cell lines in which kinase target reached statistical significance versus negative siRNA control. Differential viability (top); caspase-3/7–dependent apoptosis (bottom).

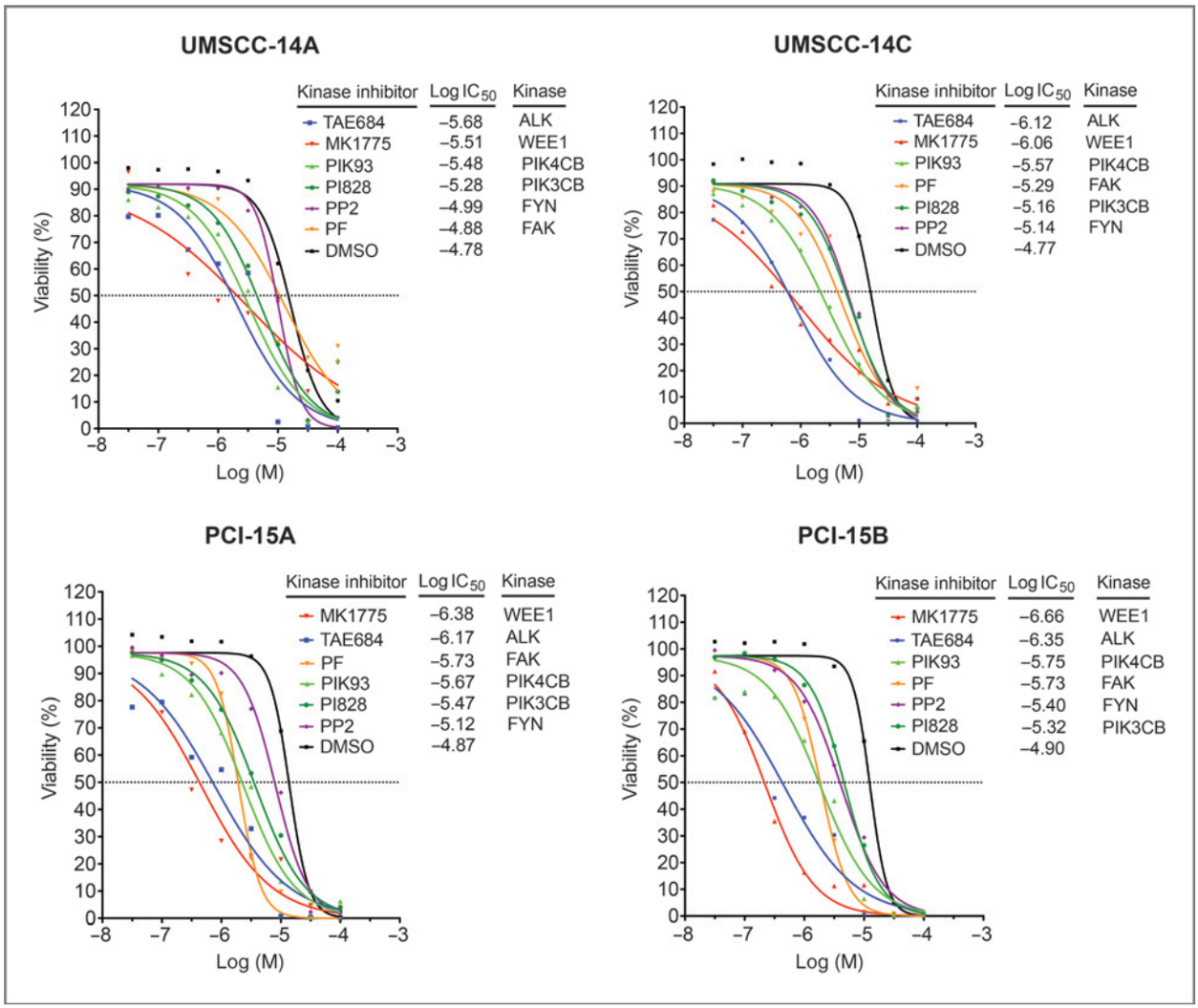

Figure 3. Chemical inhibition of SRC family kinase (FYN), phosphatidylinositiol kinases (PIK3CB, PIK4CB), focal adhesion kinase (FAK), tyrosine kinase receptor (ALK), and G_2–M mitotic kinase (WEE1) impair viability of autologous pairs of p53-mutant HNSCC cells. Dose–response curves performed with six kinase inhibitors (MK-1775, TAE684, PF-562271, PI828, PIK93, and PP2) against kinase targets (WEE1, ALK, PIK3CB, PIK4CB, FYN, and FAK; 8-point, mean ($N = 3$), range 100 μmol/L to 30 nmol/L, $R^2 > 0.85$ for all curves. Autologous HNSCC cell pairs (UMSCC-14A, UMSCC-14C, PCI-15A, and PCI-15B) derived from primary and recurrent/metastatic site from the same patient (14, 15).

MSCC cells compared with *p53* wild-type cells (0.22 vs. 4.5 μmol/L; Fig. 4A). The IC_{50} for MK-1775 in p53-mutant PCI-15A and PCI-15B HNSCC cells (0.14–0.17 μmol/L) and p53 wild-type SCC-61 and UMSCC-17A cells (2.8–4.5 μmol/L) showed a similar differential sensitivity to MK-1775 as the mouse SCC cells. Interestingly, the HPV^+, p53 wild-type UMSCC-47, UPCI:SCC090, and UMSCC104 cells showed IC_{50} values (0.29–0.84 μmol/L) closer to p53-mutant cell lines (Fig. 4B and C).

As WEE1 regulates mitotic entry, this suggests p53-deficient cells are sensitive to deregulation of the G_2–M transition. CHK1, a kinase required for the DNA damage induced G_2–M checkpoint, and AURKA, a kinase involved in spindle assembly during mitosis, were also identified as putative survival kinases (Fig. 2). Consistent with the WEE1 inhibitor results, p53-deficient MSCC cells were also more sensitive to the CHK1 inhibitor, AZD7762 than p53 wild-type cells (IC_{50} 0.13 vs. 2.2 μmol/L; Fig. 4A).

Data from the Genomics of Drug Sensitivity project contain dose–response measurements on 820 genomically characterized cancer cell lines treated with 138 different compounds (26). One compound in this collection, labeled 681640, is a dual WEE1/CHK1 inhibitor (27). We used mutational profiling data from the Sanger Cancer Cell Line Project to classify cell lines based on p53 mutational status and tested for correlation with sensitivity to 681640 (Supplementary Table S21; ref. 28). Examination of the 42 cells that were derived from SCCs of the head and neck (19), esophagus (11), lung (five), cervix (three), vulva (three), and skin (one), showed that, despite a broad range of

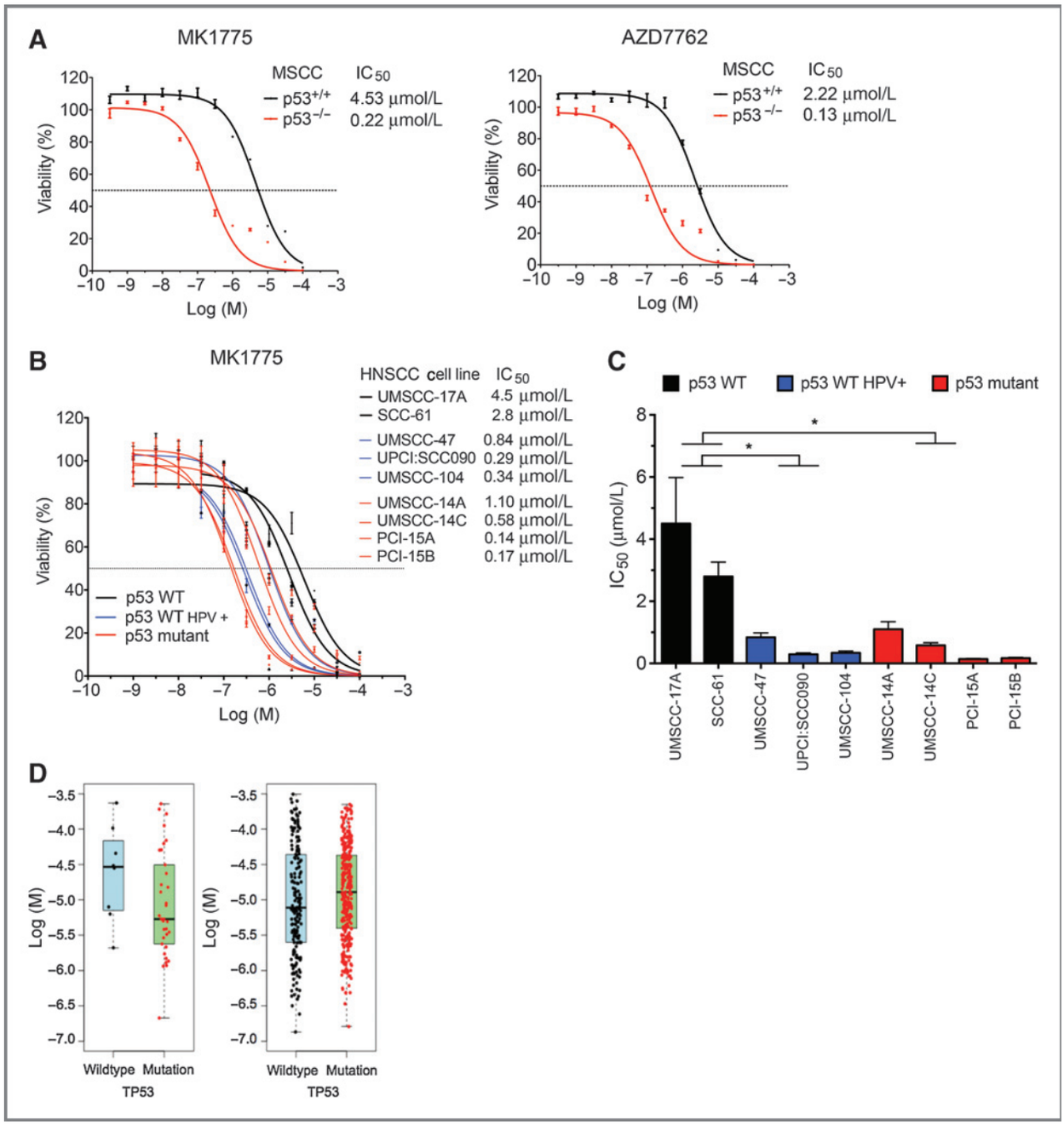

Figure 4. Drug sensitivity of MSCC and HNSCC cells to chemical inhibition of G_2–M mitotic kinases determined by loss-of-function mutational status of p53. A, differential sensitivity of MSCC $p53^{+/+}$ and $p53^{-/-}$ cells to the WEE1 inhibitor MK-1775 and CHK1/CHK2 inhibitor AZD7762. Of note, 12-point dose–response curves, mean ± SEM ($N = 3$), range, 100 μmol/L–0.3 nmol/L, $R^2 > 0.95$ for all curves. B, differential sensitivity of HNSCC cell lines to MK-1775. Eight and 11-point dose–response curves, mean ± SEM ($N = 3$–4), range 100 mmol/L to 1 nmol/L, $R^2 > 0.86$ for all curves. C, bar graph of MK-1775 IC_{50} values for each of the nine cell lines. *, statistically significant differences in IC_{50} values between p53 wild-type (WT) versus either p53 wild-type, HPV(+) or p53-mutant HNSCC cell lines, ANOVA with the Holm–Sidak posttest;*, $P < 0.05$. D, box plots of TP53 mutation status versus IC_{50} values following treatment with the dual WEE1/CHK1 inhibitor 681640 based on data from the Genomics of Drug Sensitivity project. Left, comparison of TP53 wild-type ($n = 8$) and TP53-mutant ($n = 34$) SCC cells. Right, comparison of TP53 wild-type ($n = 177$) and TP53-mutant ($n = 322$) status across all cell lines excluding SCC lines, representing a diversity of tumor types.

sensitivities in both wild-type and mutant groups, on average p53-mutant SCC cells had increased sensitivity to 681640 compared with p53 wild-type cells (median IC_{50}, 5.34 vs. 29.23 μmol/L; $P = 0.005$; Fig. 4D). However, the correlation between p53 status and sensitivity to 681640 was not observed in the overall collection of 499 cell lines,

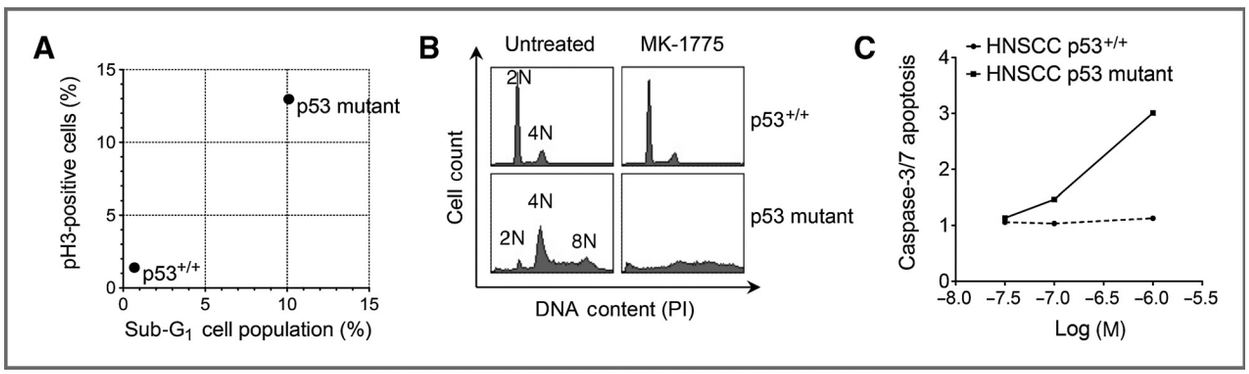

Figure 5. MK-1775 induces mitotic entry, polyploidy, and apoptosis in HNSCC p53-mutant cells. A, flow cytometric analysis of HNSCC $p53^{+/+}$ (UM-SCC17A) and p53-mutant (PCI-15B) cells showing the percentage of mitotic cells at 8 hours after MK-1775 treatment (*y*-axis) versus the percentage of cell death at 24 hours (*x*-axis) normalized to untreated cells. B, cell-cycle profiles at 24 hours after MK-1775 treatment demonstrates abrogation of G2 (4N) cell population and generation of polyploidy in p53-mutant cells. C, caspase-3/7–dependent apoptosis in HNSCC $p53^{+/+}$ and HNSCC p53-mutant cells over 48 hours at three different concentrations (30 nmol/L, 100 nmol/L, and 1 μmol/L) of MK-1775 (*x*-axis); the fold change AUC ratio, AUC (MK-1775)/AUC (vehicle) (*y*-axis).

which excluded the 42 SCC cell lines and represents a broader variety of tumor types. In fact, the trend between p53-mutant status and 681640 sensitivity was reversed (median IC_{50}, 12.83 vs. 7.75 μmol/L; $P = 1.348 \times 10^{-5}$; Fig. 4D). This analysis emphasizes the importance of validating candidate synthetic lethal interactions or drug sensitivities in specific tumor contexts and it indicates that other factors besides p53 mutational status affect sensitivity to 681640.

We next used flow cytometric cell-cycle analysis to determine the basis for the enhanced sensitivity of p53-mutant SCC cells to WEE1 inhibition. Treatment of cells with MK-1775 led to unscheduled mitotic entry in p53 mutant but not wild-type cells as measured by phospho-histone H3 (serine 10) (Fig. 5A). This was accompanied by an increase in sub-G_1 DNA content, a loss of 4N DNA content, and activation of the apoptotic marker, caspase-3/7 (Fig. 5B and C). This indicates that WEE1 inhibition by MK-1775 in p53-mutant SCC cells caused unscheduled mitotic entry leading to mitotic catastrophe and apoptotic cell death.

To determine whether WEE1 inhibition was effective against p53-mutant HNSCC in a preclinical tumor model, we performed a four-arm double-blind study on PCI-15B xenograft-bearing mice. On the basis of our previous research PCI-15B demonstrates high metastatic potential as determined by cell migration and anchorage-independent growth assays, as well as the ability to metastasize to lymph nodes in an orthotopic mouse model of HNSCC (9). In addition, the PCI-15B line is also relatively resistant to cisplatin and radiation (data not shown). When tumors reached a palpable mass of >50 mm^3, mice were randomized into four treatment arms and treated with vehicle, MK-1775, cisplatin, or cisplatin plus MK-1775. Cisplatin is the standard chemotherapeutic agent for HNSCC and cisplatin plus MK-1775 was used to determine whether inhibition of WEE1 would synergize with DNA-damaging therapy, as p53-mutant tumor cells would be expected to depend on G_2–M arrest after DNA-damaging treatment to repair DNA. Twice weekly oral gavage of MK-1775 inhibited growth of HNSCC tumors by 66% over the 4-week protocol as compared with vehicle (Fig. 6A and B, $P = 0.06$). Cisplatin alone led to partial tumor regression, but also caused significant weight loss (Supplementary Fig. S4). However, MK-1775 given 24 hours after cisplatin therapy further augmented tumor regression (60% reduction with cisplatin alone vs. 80% reduction with cisplatin plus MK-1775, $P = 0.003$). Tumor lysates from MK-1775–treated mice probed with WEE1 and CDC2 antibodies showed reduced phosphorylation of WEE1 and its substrate CDC2, indicating that oral administration of MK-1775 effectively blocked WEE1 kinase activity in tumors (Fig. 6C and D).

Discussion

One of the most significant clinical challenges in the management of patients with HNSCC is recurrent disease. In addition to being resistant to radio- or chemotherapy, these tumors can present with distant metastases, leaving palliative care as the only option. Here, we applied a functional kinomic approach to identify new candidate therapeutic targets for aggressive p53-mutant tumors. To prioritize targets, we also screened isogenic murine SCC cells with germline mutations (*Atm*, *DNA-PKcs*, *p19Arf*, and *Trp53*) in the p53 pathway. The rationale for this cross-species analysis was to identify evolutionary conserved survival pathways/kinases, the inhibition of which was associated with loss of cellular viability in p53-mutant cells. Retesting of these prioritized targets with independent siRNAs using both viability and apoptosis endpoints identified those that were effective in most or all cells tested, as well as those that were cell line or condition specific.

Comparing siRNA kinome screening results from cells derived from primary and recurrent/metastatic lesions revealed a high degree of concordance, implying that tumor cells isolated at different times or locations from the same patient share common vulnerabilities. In addition, recurrent/metastatic cell lines tended to be less responsive to kinase knockdown relative to cells from

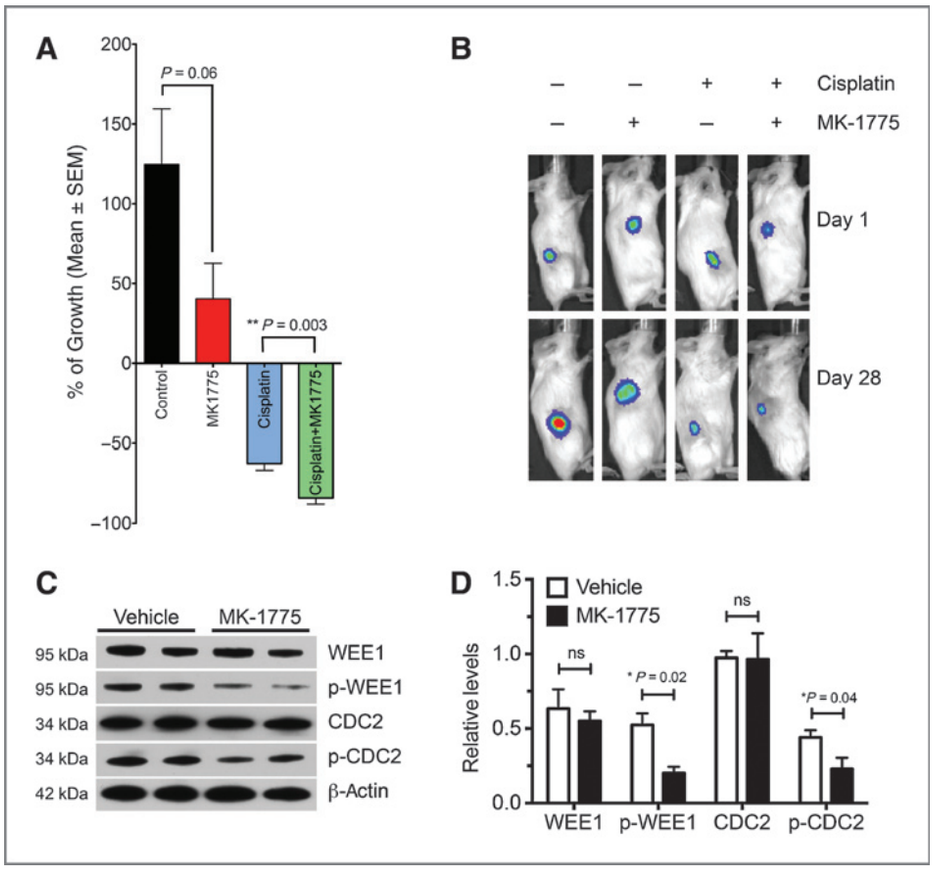

Figure 6. WEE1 inhibitor MK-1775 potentiates the efficacy of cisplatin in established p53-mutant HNSCC xenografts. A, the percentage growth of PCI-15B xenografts in mice treated with MK-1775 and/or cisplatin. The *y*-axis, the percentage of change (mean ± SEM) in tumor volume over the course of a 4-week protocol for each group; $n = 7$ per group; unpaired *t* tests; control versus MK1775, $P = 0.06$; cisplatin versus cisplatin plus MK1775; **, $P = 0.003$. B, bioluminescence images of a representative tumor-bearing mouse from each group at start (day 1) and end of protocol (day 28). C, immunoblot analysis of xenograft tumor lysates from two vehicle and two MK-1775–treated mice with specific antibodies to WEE1 kinase substrates: p-CDC2, CDC2, p-WEE1, WEE1, and β-actin loading control. D, bar graph of relative protein levels of immunoblot analysis for WEE1, p-WEE1, CDC2, p-CDC2, mean ± SD; normalized values for vehicle versus MK1775 were compared via the unpaired *t* test, $P < 0.05$ as significant; $n = 2$; WEE1, ns; p-WEE1; *, $P = 0.02$ (one-tail); CDC2, ns; p-CDC2; *, $P = 0.04$ (one-tail).

the primary lesion, suggesting development of resistance to target knockdown induced cell death. Altogether, these findings indicate this functional kinomic platform can reliably identify profiles of essential survival kinases specific to individual patients.

To further validate candidate therapeutic targets, we tested several small-molecule kinase inhibitors as a confirmatory step to support the RNAi results as well as to identify those inhibitors that might be effective for testing *in vivo*. Overall, this strategy identified the WEE1 kinase for further validation *in vivo* as RNAi-mediated knockdown of WEE1 led to a significant reduction in cell viability and a concomitant increase in apoptosis in all nine HNSCC cell lines tested. Moreover, p53-deficient MSCC and HNSCC cells were highly sensitive to the specific WEE1 inhibitor MK-1775 relative to p53 wild-type cells, a finding that has been observed in other settings (29–31). Furthermore, the HPV^+ p53 wild-type cell lines were more sensitive to MK-1775 than the p53 wild-type cell lines, consistent with the idea that functional loss of p53, either by the E6 viral component of HPV or by somatic mutation is associated with greater sensitivity to the WEE1 inhibitor, MK1775 (Fig. 4C). Mechanistically, WEE1 inhibition in p53-mutant cells, but not wild-type cells, led to unscheduled mitotic entry, mitotic catastrophe, and apoptosis, consistent with previous reports (24, 32). The G_2 checkpoint kinase CHK1 was also a top candidate from our screen and p53-deficient SCC cells showed an increased sensitivity to both a CHK1 and a dual WEE1/CHK1 inhibitor. Collectively, this suggests p53-deficient SCC cells may be particularly vulnerable to deregulation of the G_2–M transition.

As preclinical validation, we demonstrated that oral administration of MK-1775 inhibited the growth of p53-mutant HNSCC xenografts and also cooperated with cisplatin to induce tumor regression. This xenograft protocol was designed and implemented after careful examination of previous preclinical studies using genotoxic agents and/or MK-1775, and it was determined that the greatest responses to the WEE1 inhibitor MK-1775 would likely be obtained in p53-mutant HNSCC when given after genotoxic treatment (i.e., cisplatin; refs. 29–31). Our comparably conservative MK-1775 dosing regimen of two times per week, 24 hours pre- and post-cisplatin treatment was performed in the context of limiting potential toxicities from cisplatin treatment. Given that this current regimen was well tolerated as evidenced in Supplementary Fig. S4 (body weight of MK-1775–treated mice), it is quite possible that higher doses of the MK-1775 inhibitor would also be well tolerated and high efficacy could be attained either as a single-agent or in combination with genotoxic treatment.

Currently, cisplatin chemotherapy for the treatment of HNSCC is given either in the neoadjuvant setting or

concurrently with radiotherapy. Unfortunately, the associated toxicities of combining cisplatin with other chemotherapeutic agents or the three potentially toxic cisplatin doses of 100 mg/m^2 administered during radiation treatment can limit the clinical applicability of these regimens. Thus, the degree by which MK-1775 enhances response to cisplatin would not only increase the effectiveness of existing therapy, but would open the possibility of reducing cisplatin dosing to minimize side-effects and broaden patient candidacy to these regimens.

MK-1775 has been shown to sensitize other p53-mutant tumors to DNA-damaging agents (30, 31, 33). Molecular analysis of HNSCC tumor lysates showed reduced phosphorylation of the WEE1 substrate CDC2, indicating that MK-1775 inhibited its intended target. We previously found amplification of 11q13.1 in metastatic HNSCC tumor cells with corresponding overexpression of cyclin B, the activating subunit of CDC2 (34), which could exacerbate the sensitivity of HNSCC cells to WEE1 inhibition.

In addition to WEE1 and CHK1, siRNAs to other mitotic kinases, including AURKA and NEK4, reduced viability and increased apoptosis in the majority of HNSCC cells, including those derived from recurrent/metastatic lesions, suggesting potential as therapeutic targets. AURKA and CHK1 are being pursued as drug targets (35–37), whereas NEK4 a member of the NIMA family of kinases modulates sensitivity to microtubule poisons and DNA damage (38–40).

siRNAs to several Src family kinases (SFK) or related signaling proteins (FYN, TXK, and CAM2KB) also reduced viability in one or more HNSCC cell lines and were prioritized as candidates in the cross species comparisons. FYN is an SFK involved in many prooncogenic processes such as cellular proliferation, integrin-mediated and PI3K signaling, and TXK is a tyrosine kinase activated by the SRC family kinase LYN (41–43). SFKs are activated by mitogenic signals to induce HNSCC cell proliferation and LYN mediates cell motility and tumor growth in head and neck cancer (43, 44). Furthermore, SRC/FAK signaling correlates strongly with phenotypes associated with tumor progression such as invasion and metastasis (44, 45) and FAK (focal adhesion kinase) itself is amplified in HNSCC (48), providing further support for targeting the SFK pathway in more aggressive subtypes of HNSCC (49, 50).

In summary, our cross-species functional kinomic approach using autologous pairs of primary and recurrent/metastatic p53-mutant HNSCC lines, coupled with isogenic mouse SCC cells with defined mutations along the p53 pathway has identified several survival kinases as candidate therapeutic targets for aggressive HNSCC. These kinases regulate a range of cellular processes such as phosphatidylinositol, focal adhesion, and Src signaling pathways, and the G_2–M cell-cycle transition, suggesting functional targets for therapeutic intervention. Discovery and development of multiple targets may prove to be a useful strategy, as tumors frequently develop resistance to single agents and targeting multiple vulnerabilities simultaneously may be a required to achieve long-term remission.

Our preclinical data on WEE1 illustrate not only the vulnerabilities of p53-mutant HNSCC cells to deregulation of the G_2–M transition, but also support the initiation of clinical trials with MK-1775 or other G_2–M checkpoint inhibitors for HNSCC, particularly in combination with cisplatin. More generally, this study illustrates the utility of integrating functional genomic approaches with more traditional descriptive genomic and molecular profiles to identify therapeutic targets in cancer.

Disclosure of Potential Conflicts of Interest

W.G. Yarbrough reports receiving a commercial research grant from AbbVie. No potential conflicts of interest were disclosed by the other authors.

Authors' Contributions

Conception and design: R. Moser, C. Xu, C.J. Kemp, E. Méndez
Development of methodology: R. Moser, C. Xu, M. Kao, J. Annis, K.E. Gurley, A. Biktasova, C. Grandori, C.J. Kemp, E. Méndez
Acquisition of data (provided animals, acquired and managed patients, provided facilities, etc.): R. Moser, C. Xu, M. Kao, J. Annis, L.A. Lerma, C.M. Schaupp, K.E. Gurley, W.G. Yarbrough, C.J. Kemp, E. Méndez
Analysis and interpretation of data (e.g., statistical analysis, biostatistics, computational analysis): R. Moser, C. Xu, M. Kao, L.A. Lerma, C.M. Schaupp, I.S. Jang, A. Biktasova, W.G. Yarbrough, A.A. Margolin, C. Grandori, C.J. Kemp, E. Méndez
Writing, review, and/or revision of the manuscript: R. Moser, C. Xu, M. Kao, L.A. Lerma, I.S. Jang, A. Biktasova, A.A. Margolin, C. Grandori, C.J. Kemp, E. Méndez
Administrative, technical, or material support (i.e., reporting or organizing data, constructing databases): R. Moser, L.A. Lerma, E. Méndez
Study supervision: R. Moser, A.A. Margolin, C.J. Kemp, E. Méndez
Developed standardized automation platform for functional genomics from factorial feasibility through modifier screening: J. Annis

Acknowledgments

The authors thank Natalia Isaeva for her technical support with MK-1775 dose–response experiments.

Grant Support

This work was supported by two FHCRC/UW Cancer Consortium Pilot grants from the NIH (P30CA015704); the National Center for Research Resources (5KL2RR025015); the Howard Hughes Medical Institute Early Physician-Scientist Career Development Award; American Cancer Society grant (RSG TBG-123653); the Mouse Models of Human Cancer Consortium (U01 CA141550); the National Institute of Environmental Health Science (ES020116); the Integrated Cancer Biology Program (54CA149237); National Cancer Institute grant (U01 CA176303); and center funds from the Department of Otolaryngology/Head and Neck Surgery at the University of Washington and VA Puget Sound Health Care System

The costs of publication of this article were defrayed in part by the payment of page charges. This article must therefore be hereby marked *advertisement* in accordance with 18 U.S.C. Section 1734 solely to indicate this fact.

Received November 19, 2013; revised March 18, 2014; accepted March 19, 2014; published online August 14, 2014.

References

1. Bernier J, Domenge C, Ozsahin M, Matuszewska K, Lefebvre JL, Greiner RH, et al. Postoperative irradiation with or without concomitant chemotherapy for locally advanced head and neck cancer. N Engl J Med 2004;350:1945–52.

2. Machtay M, Moughan J, Trotti A, Garden AS, Weber RS, Cooper JS, et al. Factors associated with severe late toxicity after concurrent chemoradiation for locally advanced head and neck cancer: an RTOG analysis. J Clin Oncol 2008;26:3582–9.
3. Bonner JA, Harari PM, Giralt J, Azarnia N, Shin DM, Cohen RB, et al. Radiotherapy plus cetuximab for squamous-cell carcinoma of the head and neck. N Engl J Med 2006;354:567–78.
4. Gasco M, Crook T. The p53 network in head and neck cancer. Oral Oncol 2003;39:222–31.
5. Hauser U, Balz V, Carey TE, Grenman R, Van Lierop A, Scheckenbach K, et al. Reliable detection of p53 aberrations in squamous cell carcinomas of the head and neck requires transcript analysis of the entire coding region. Head Neck 2002;24:868–73.
6. Muller PA, Vousden KH, Norman JC. p53 and its mutants in tumor cell migration and invasion. J Cell Biol 2011;192:209–18.
7. Poeta ML, Manola J, Goldwasser MA, Forastiere A, Benoit N, Califano JA, et al. TP53 mutations and survival in squamous-cell carcinoma of the head and neck. N Engl J Med 2007;357:2552–61.
8. Skinner HD, Sandulache VC, Ow TJ, Meyn RE, Yordy JS, Beadle BM, et al. TP53 disruptive mutations lead to head and neck cancer treatment failure through inhibition of radiation-induced senescence. Clin Cancer Res 2012;18:290–300.
9. Xu C, Wang P, Liu Y, Zhang Y, Fan W, Upton MP, et al. Integrative genomics in combination with RNA interference identifies prognostic and functionally relevant gene targets for oral squamous cell carcinoma. PLoS Genet 2013;9:e1003169.
10. Bailey SL, Gurley KE, Hoon-Kim K, Kelly-Spratt KS, Kemp CJ. Tumor suppression by p53 in the absence of Atm. Mol Cancer Res 2008;6:1185–92.
11. Kelly-Spratt KS, Gurley KE, Yasui Y, Kemp CJ. p19Arf suppresses growth, progression, and metastasis of Hras-driven carcinomas through p53-dependent and -independent pathways. PLoS Biol 2004;2:E242.
12. Kemp CJ, Donehower LA, Bradley A, Balmain A. Reduction of p53 gene dosage does not increase initiation or promotion but enhances malignant progression of chemically induced skin tumors. Cell 1993;74:813–22.
13. Kemp CJ, Vo K, Gurley KE. Resistance to skin tumorigenesis in DNAPK-deficient SCID mice is not due to immunodeficiency but results from hypersensitivity to TPA-induced apoptosis. Carcinogenesis 1999;20:2051–6.
14. Zhao M, Sano D, Pickering CR, Jasser SA, Henderson YC, Clayman GL, et al. Assembly and initial characterization of a panel of 85 genomically validated cell lines from diverse head and neck tumor sites. Clin Cancer Res 2011;17:7248–64.
15. Ise K, Nakamura K, Nakao K, Shimizu S, Harada H, Ichise T, et al. Targeted deletion of the H-ras gene decreases tumor formation in mouse skin carcinogenesis. Oncogene 2000;19:2951–6.
16. Kemp CJ. Multistep skin cancer in mice as a model to study the evolution of cancer cells. Semin Cancer Biol 2005;15:460–73.
17. Ku TK, Nguyen DC, Karaman M, Gill P, Hacia JG, Crowe DL. Loss of p53 expression correlates with metastatic phenotype and transcriptional profile in a new mouse model of head and neck cancer. Mol Cancer Res 2007;5:351–62.
18. Ruddell A, Kelly-Spratt KS, Furuya M, Parghi SS, Kemp CJ. p19/Arf and p53 suppress sentinel lymph node lymphangiogenesis and carcinoma metastasis. Oncogene 2008;27:3145–55.
19. Wang YV, Leblanc M, Wade M, Jochemsen AG, Wahl GM. Increased radioresistance and accelerated B-cell lymphomas in mice with Mdmx mutations that prevent modifications by DNA damage–activated kinases. Cancer Cell 2009;16:33–43.
20. Kiyono T, Foster SA, Koop JI, McDougall JK, Galloway DA, Klingelhutz AJ. Both Rb/p16INK4a inactivation and telomerase activity are required to immortalize human epithelial cells. Nature 1998;396:84–8.
21. Toyoshima M, Howie HL, Imakura M, Walsh RM, Annis JE, Chang AN, et al. Functional genomics identifies therapeutic targets for MYC-driven cancer. Proc Natl Acad Sci U S A 2012;109:9545–50.
22. Zhang JH, Chung TD, Oldenburg KR. A simple statistical parameter for use in evaluation and validation of high-throughput screening assays. J Biomol Screen 1999;4:67–73.
23. Birmingham A, Selfors LM, Forster T, Wrobel D, Kennedy CJ, Shanks E, et al. Statistical methods for analysis of high-throughput RNA interference screens. Nat Methods 2009;6:569–75.
24. Aarts M, Sharpe R, Garcia-Murillas I, Gevensleben H, Hurd MS, Shumway SD, et al. Forced mitotic entry of S-phase cells as a therapeutic strategy induced by inhibition of WEE1. Cancer Discov 2012;2:524–39.
25. Jackson AL, Bartz SR, Schelter J, Kobayashi SV, Burchard J, Mao M, et al. Expression profiling reveals off-target gene regulation by RNAi. Nat Biotechnol 2003;21:635–7.
26. Garnett MJ, Edelman EJ, Heidorn SJ, Greenman CD, Dastur A, Lau KW, et al. Systematic identification of genomic markers of drug sensitivity in cancer cells. Nature 2012;483:570–5.
27. Palmer BD, Thompson AM, Booth RJ, Dobrusin EM, Kraker AJ, Lee HH, et al. 4-Phenylpyrrolo[3,4-c]carbazole-1,3(2H,6H)-dione inhibitors of the checkpoint kinase Wee1. Structure-activity relationships for chromophore modification and phenyl ring substitution. J Med Chem 2006;49:4896–911.
28. Forbes SA, Bindal N, Bamford S, Cole C, Kok CY, Beare D, et al. COSMIC: mining complete cancer genomes in the Catalogue of Somatic Mutations in Cancer. Nucleic Acids Res 2011;39:D945–50.
29. Hirai H, Iwasawa Y, Okada M, Arai T, Nishibata T, Kobayashi M, et al. Small-molecule inhibition of Wee1 kinase by MK-1775 selectively sensitizes p53-deficient tumor cells to DNA-damaging agents. Mol Cancer Ther 2009;8:2992–3000.
30. Bridges KA, Hirai H, Buser CA, Brooks C, Liu H, Buchholz TA, et al. MK-1775, a novel Wee1 kinase inhibitor, radiosensitizes p53-defective human tumor cells. Clin Cancer Res 2011;17:5638–48.
31. Rajeshkumar NV, De Oliveira E, Ottenhof N, Watters J, Brooks D, Demuth T, et al. MK-1775, a potent Wee1 inhibitor, synergizes with gemcitabine to achieve tumor regressions, selectively in p53-deficient pancreatic cancer xenografts. Clin Cancer Res 2011;17:2799–806.
32. De Witt Hamer PC, Mir SE, Noske D, Van Noorden CJ, Wurdinger T. WEE1 kinase targeting combined with DNA-damaging cancer therapy catalyzes mitotic catastrophe. Clin Cancer Res 2011;17:4200–7.
33. Hirai H, Arai T, Okada M, Nishibata T, Kobayashi M, Sakai N, et al. MK-1775, a small-molecule Wee1 inhibitor, enhances anti-tumor efficacy of various DNA-damaging agents, including 5-fluorouracil. Cancer Biol Ther 2010;9:514–22.
34. Xu C, Liu Y, Wang P, Fan W, Rue TC, Upton MP, et al. Integrative analysis of DNA copy number and gene expression in metastatic oral squamous cell carcinoma identifies genes associated with poor survival. Mol Cancer 2010;9:143.
35. Dar AA, Goff LW, Majid S, Berlin J, El-Rifai W. Aurora kinase inhibitors–rising stars in cancer therapeutics? Mol Cancer Ther 2010;9:268–78.
36. Katayama H, Sen S. Aurora kinase inhibitors as anticancer molecules. Biochim Biophys Acta 2010;1799:829–39.
37. Ma CX, Janetka JW, Piwnica-Worms H. Death by releasing the breaks: CHK1 inhibitors as cancer therapeutics. Trends Mol Med 2011;17:88–96.
38. Doles J, Hemann MT. Nek4 status differentially alters sensitivity to distinct microtubule poisons. Cancer Res 2010;70:1033–41.
39. Moniz L, Dutt P, Haider N, Stambolic V. Nek family of kinases in cell cycle, checkpoint control, and cancer. Cell Div 2011;6:18.
40. Nguyen CL, Possemato R, Bauerlein EL, Xie A, Scully R, Hahn WC. Nek4 regulates entry into replicative senescence and the response to DNA damage in human fibroblasts. Mol Cell Biol 2012;32:3963–77.
41. Xi S, Zhang Q, Dyer KF, Lerner EC, Smithgall TE, Gooding WE, et al. Src kinases mediate STAT growth pathways in squamous cell carcinoma of the head and neck. J Biol Chem 2003;278:31574–83.
42. Debnath J, Chamorro M, Czar MJ, Schaeffer EM, Lenardo MJ, Varmus HE, et al. rlk/TXK encodes two forms of a novel cysteine string tyrosine kinase activated by Src family kinases. Mol Cell Biol 1999;19:1498–507.
43. Mano H, Yamashita Y, Miyazato A, Miura Y, Ozawa K. Tec protein-tyrosine kinase is an effector molecule of Lyn protein–tyrosine kinase. FASEB J 1996;10:637–42.

44. Wheeler SE, Morariu EM, Bednash JS, Otte CG, Seethala RR, Chiosea SI, et al. Lyn kinase mediates cell motility and tumor growth in EGFRvIII-expressing head and neck cancer. Clin Cancer Res 2012;18:2850–60.
45. Zhang Q, Thomas SM, Xi S, Smithgall TE, Siegfried JM, Kamens J, et al. SRC family kinases mediate epidermal growth factor receptor ligand cleavage, proliferation, and invasion of head and neck cancer cells. Cancer Res 2004;64:6166–73.
46. Matsumoto T, Jiang J, Kiguchi K, Ruffino L, Carbajal S, Beltran L, et al. Targeted expression of c-Src in epidermal basal cells leads to enhanced skin tumor promotion, malignant progression, and metastasis. Cancer Res 2003;63:4819–28.
47. McLean GW, Carragher NO, Avizienyte E, Evans J, Brunton VG, Frame MC. The role of focal-adhesion kinase in cancer—a new therapeutic opportunity. Nat Rev Cancer 2005;5:505–15.
48. Agochiya M, Brunton VG, Owens DW, Parkinson EK, Paraskeva C, Keith WN, et al. Increased dosage and amplification of the focal adhesion kinase gene in human cancer cells. Oncogene 1999;18:5646–53.
49. Egloff AM, Grandis JR. Targeting epidermal growth factor receptor and SRC pathways in head and neck cancer. Semin Oncol 2008;35:286–97.
50. Stabile LP, He G, Lui VW, Henry C, Gubish CT, Joyce S, et al. c-Src activation mediates erlotinib resistance in head and neck cancer by stimulating c-Met. Clin Cancer Res 2013;19:380–92.